Combustion and Flame 162 (2015) 3503–3515

Contents lists available at ScienceDirect

Combustion and Flame

journal homepage: www.elsevier.com/locate/combustflame

Chemical looping dechlorination through adsorbent-decorated Fe_2O_3/Al_2O_3 oxygen carriers

Jinxing Wang, Haibo Zhao*

State Key Laboratory of Coal Combustion, Huazhong University of Science and Technology, Wuhan 430074, PR China

ARTICLE INFO

Article history:
Received 27 February 2015
Revised 8 June 2015
Accepted 8 June 2015
Available online 20 July 2015

Keywords:
Chemical looping combustion
Dechlorination
Adsorbent
PCDD/Fs
Fe_2O_3/Al_2O_3

ABSTRACT

Plastic waste incineration is the main source of polychlorinated dibenzo-p-dioxins and dibenzofurans (PCDD/Fs), which, as toxic materials, have aroused increasing attention all over the world. Based on the formation mechanisms of PCDD/Fs, the key approaches to eliminate PCDD/Fs are to maintain an oxygen-deficient atmosphere to suppress the de novo route of PCDD/Fs formation and to constrain the presence of free chlorine to prevent the formation of PCDD/Fs from the conversion of precursors (e.g., unchlorinated benzene and phenol). Chemical looping combustion (CLC), which utilizes active lattice oxygen provided by an oxygen carrier (OC) for fuel oxidation in the absence of O_2 was, for the first time, proposed as a promising pattern for disposing plastic waste. To constrain the presence of free chlorine, the feasibility of dechlorination through adsorbent-decorated Fe-based OC during the CLC process was investigated through thermodynamic simulation, isothermal kinetic experiments in a thermogravimentric analyzer (TGA), and batch fluidized bed reactor experiments. For three $CaO/K_2O/Na_2O$ adsorbents, CaO decoration for OC particles exhibits the highest dechlorination efficiency, however it results in the maximum activation energy in the TGA experiments and relatively more carbon deposition on the OC particles in these batch fluidized bed experiments. Subsequently, the effects of the CaO decoration method (wet impregnation, coprecipitation, and physical mixture), CaO loading and reaction temperature on the efficiencies of dechloridation and combustion were investigated in the batch fluidized bed reactor that simulates a real chemical looping process. The results indicated that the wet impregnation method demonstrates the best adsorbent decoration and that 5 wt% CaO loading reaches an optimized level of dechloridation. In addition, increasing the temperature can improve the dechlorination, but it also increases carbon deposition, leading to a lower combustion efficiency. Next, the dechloridation efficiency gradually descends, and correspondingly, the mole ratio between Ca and Fe on the OC particle surface exhibits a declining trend with an increase in the cycle number; these results were verified by ion chromatography and an environmental scanning electron microscope coupled with energy dispersive X-ray spectroscopy (ESEM-EDX), respectively. Notably, the ESEM-EDX result demonstrates the accumulation of Cl elements onto the surface of OC particles. Last, the reduced samples were washed using a dilute hydrochloric acid solution after 30 cycles, and the ESEM-EDX result demonstrates the removal of the Ca and Cl elements from the surface of these OC particles and the regeneration of these OC particles. Overall, these results provide sound evidence for the feasibility of chemical looping dechlorination through the use of adsorbent-decorated Fe_2O_3/Al_2O_3 OC particles.

1. Introduction

Accelerated industrial development and enhanced living standards have led to a rapid increase in the generation of plastic wastes, including medical plastics [1]. These medical plastics are characterized by their toxic and infectious nature and have the potential to cause health risks and environmental pollution without proper treatment and management [2]. Consequently, the disposal of these plastic wastes has become a serious problem, which China, as well as many countries, is currently confronting [3]. Traditionally, the destruction of these wastes via landfill deposition is regarded as the preferred treatment option. However, the use of landfills for the disposal of plastic waste leads to problems. First, a considerable amount of space is required because the volume of plastics waste cannot be compacted. Additionally, landfills pose a potential danger because of the possibility of accidental fires with high emissions of hazardous gases [4]. In addition, pathogens and organic contaminants cannot be destroyed. Hence, the use of a landfill for medical plastics is not acceptable under current international policy [5]. To overcome these issues, incineration has been demonstrated to be a fast and

* Corresponding author. Fax: +86 27 8754 5526.
E-mail address: klinsmannzhb@163.com, hzhao@mail.hust.edu.cn (H. Zhao).

http://dx.doi.org/10.1016/j.combustflame.2015.06.008
0010-2180/

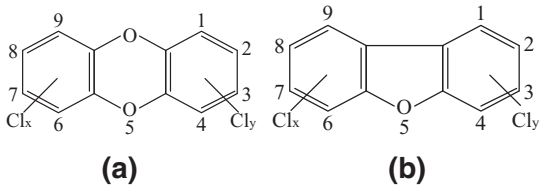

Fig. 1. Molecular structure of polychlorinated dibenzo-*p*-dioxins (a) and dibenzofurans (b).

commercially available technology for solid waste treatment because it possesses the advantages of pathogen destruction, volume reduction (approximately 90%), weight reduction (approximately 70%), toxicity reduction and energy recovery relative to the use of landfills [6]. In addition, the waste-to-energy conversion of plastic wastes has been viewed as an important practice to relieve the pressure of increasing waste generation and to act as a source of inexpensive energy [7]. Unfortunately, plastic waste incinerators can emit toxic air pollutants if the incinerators are not properly designed or operated. Pollutants include particulate matter, acid gases, trace metals, products of incomplete combustion and polynuclear organic matter. Among these pollutants, PCDD/Fs in exhaust gases are of major concern [8]. Until now, activated carbon injection (ACI) [9–11] and suppressant addition [12–14] have been widely adopted for controlling emissions of PCDD/Fs from stationary sources, including municipal waste incinerators (MWIs), to meet much more stringent emission regulations. ACI technology only transfers gaseous PCDD/Fs to the solid phase (fly ash), so further treatment is required for the disposal of fly ash that still contains relatively high level of PCDD/Fs. The addition of suppressants (calcium-based additives [15] and sulfur compounds [12]) effectively inhibits the formation of PCDD/Fs; however, the use of suppressants increases the cost. Note that these measures cannot thoroughly prohibit the emission of PCDD/Fs [15,16]. Thus, it is essential to explore effective ways to suppress the formation of PCDD/Fs based on the understanding of their formation mechanism.

PCDD/Fs are two series of aromatic polycyclic hydrocarbons that form a group of 210 different compounds consisting of 135 PCDFs and 75 PCDDs [17], as shown in Fig. 1. Two main mechanisms are involved in the formation of PCDD/Fs [18,19]: (1) the de novo synthesis of PCDDs from carbonaceous matter and polycyclic aromatic hydrocarbons at temperatures between 250 and 400 °C and (2) the formation of PCDD/Fs from the condensation reactions of precursors, such as chlorobenzenes (PCBz) and chlorophenols (POP), at temperatures between 250 and 650 °C [20]. Generally, because the precursor concentrations are relatively low, a large percentage of PCDD/Fs from incinerators are formed via the de novo route [18]. Gaseous oxygen, which can initiate carbon chain interruption and rearrangement, is considered to be one of requirements for de novo synthesis [21]. When the oxygen concentration is varied from 1% to 10%, the rate of PCDD/Fs formation obviously increases [21]. Unfortunately, in normal hazardous waste incineration processes, the O_2 concentration must remain within the range of 5% to 10% in China (GB 18484-2001) [19].

Therefore, the incineration process of plastic wastes under oxygen-deficient conditions is a potential method to suppress the formation of PCDD/Fs. Exciting, chemical-looping combustion (CLC) can meet this requirement. The CLC system is composed of two interconnected fluidized bed reactors, an air reactor (AR) and a fuel reactor (FR), as shown in Fig. 2. The fuel is introduced to the FR, where it reacts with an OC (MeO) to form CO_2 and H_2O via reaction (1). The reduced OC (Me) is transported to the AR, where it is oxidized back to its original state by air via reaction (2). The fuel never mixes with air, resulting in a stream of oxygen-depleted air from the AR and a stream of combustion products (mainly CO_2 and H_2O) from the FR [22]. If the CLC is used for disposing plastic waste, direct contact between plastic waste and air is avoided. Therefore, it is expected that

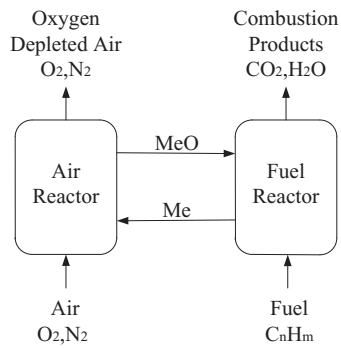

Fig. 2. Schematic description of chemical-looping combustion.

the de novo route forming PCDD/Fs can be thoroughly suppressed. In addition, several potential benefits of CLC strengthen its practical significance, including inherent CO_2 separation and low NO_x emission [23].

$$C_nH_{2m} + (2n+m)Me_xO_y \leftrightarrow nCO_2 + mH_2O + (2n+m)Me_xO_{y-1} \quad (1)$$

$$O_2 + 2Me_xO_{y-1} \leftrightarrow 2Me_xO_y \quad (2)$$

Although the de novo route for the formation of PCDD/Fs could be thoroughly suppressed during the CLC process of plastic waste, the formation of PCDD/Fs from the conversion of precursors should be effectively suppressed. The production of phenol and furan during the high-temperature disposal of solid waste could provide important precursors that can react with molecular chlorine (Cl_2) and atomic chlorine (Cl) [15] and can subsequently generate PCDD/Fs [7]. An equilibrium exists among Cl, Cl_2 and HCl [6]. In addition, HCl was detected through a thermogravimetric analyzer coupled with Fourier transform infrared spectroscopy (TG-FTIR) during the thermal degradation process of plastic waste, and the temperature interval of HCl release is 200–400 °C [24]. Generally, over 90% of the chlorine in fuel is released as HCl in the flue gas [13]. Hence, HCl removal could be a key step for suppressing the formation of PCDD/Fs. In addition, HCl itself is a hazardous pollutant that is emitted from waste incinerators because of its corrosivity [6]. To our knowledge, few papers in the literature have been reported on the adsorbent effect in the CLC process, although physical and/or chemical adsorption has been widely applied in dechlorination for conventional combustion [6,15,16]. If some adsorbents can be integrated with OC to eliminate HCl in the exhaust gas, then costly equipment and energy consumption for spraying adsorbents can be avoided; avoiding such issues is the motivation of this work.

The OC is the cornerstone of CLC technology [25]. Currently, oxides of Ni, Cu, Fe and Mn have been tested using CLC technology at different scales [26–32]. Among these commonly suggested OC materials, Fe-based OCs are believed to be the most promising for commercial CLC application because they are relatively inexpensive, readily available, and also environmentally safe compared to other metal oxides, such as NiO and CuO [33,34]. In this study, Fe_2O_3/Al_2O_3 (60 wt%/40 wt%) was synthesized using the co-precipitation method, and subsequently, three types of adsorbent (CaO, K_2O and Na_2O) and three decoration methods (wet impregnation, coprecipitation and physical mixture) were adopted for decorating these OCs. To quantify the dechlorination efficiency, synthesis gas (5.9 vol% CH_4, 21.9 vol% CO, 7.8 vol% CO_2, 12.7 vol% H_2, 1 vol% HCl and 50.7 vol% N_2) as fuel was synthesized for the dechlorination investigation. This volume ratio largely relied on the pyrolysis products of medical plastics at 900 °C. For chemical looping dechlorination (CLdeCl) through adsorbent-decorated Fe-based OC, the following questions should be addressed first. (1) Will HCl directly react with Fe-basedOC in the FR?

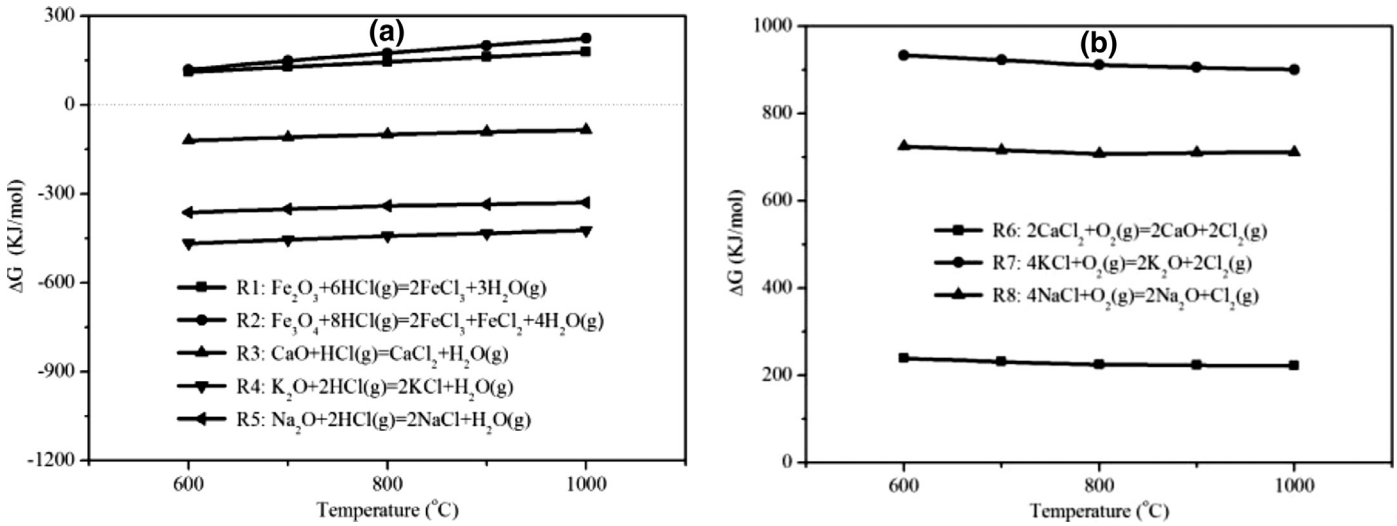

Fig. 3. Gibbs free energy of reactions for (a) Fe_xO_y and the adsorbents with HCl in the FR and (b) the corresponding chloride with O_2 in the AR.

(2) Will HCl react with adsorbents in the FR and will the corresponding chloride not react with O_2 in the AR? (3) What is the kinetics of these reactions between HCl-containing synthesis gas and adsorbent-decorated OCs? (4) Which adsorbent can be considered to be the optimal choice, and correspondingly, which decoration method should be adopted? (5) How many redox cycles of the adsorbent-decorated OC can be maintained in reactivity during the CLdeCl processes? Thermodynamic simulation, isothermal kinetic experiments, and batch fluidized bed reactor experiments were conducted to examine the feasibility of dechlorination and to analyze the effects of the adsorbent species, decoration method, loading content and reaction temperature on the efficiencies of dechlorination and combustion. This study is expected to help provide a preliminary understanding on the CLC of plastic waste using adsorbent-decorated Fe-based OC and to provide useful information on the development of the new technology for disposing plastic waste and suppressing the formation of PCDD/Fs.

2. Thermodynamic analysis

Chemical reaction thermodynamics was first used to understand the potential reaction mechanisms involved in a fuel reactor and air reactor and to choose the appropriate oxygen carriers and adsorbents [35]. The reduction reactions for Fe-based OC particles with CH_4, CO and H_2 have been investigated based on the calculation of the Gibbs free energy ($\triangle G$) [36,37]. The value of $\triangle G$ in Eq. 3 is a measure of the thermodynamic driving force that enables the reaction to proceed. The value of $\triangle G$ is related to the reaction temperature, enthalpy, and entropy through the following expression:

$$\Delta G = \Delta H - T\Delta S \tag{3}$$

where $\triangle H$ is the enthalpy, T is the absolute temperature, and $\triangle S$ is the entropy.

$\triangle G$ for any chemical reaction can be calculated from Eq. 4 as the difference between the $\triangle G$ of the products minus the $\triangle G$ of the reactions. A negative value for $\triangle G$ indicates that a reaction can proceed spontaneously without external inputs [38].

$$\Delta G = \Delta G_{\text{products}} - \Delta G_{\text{reactants}} \tag{4}$$

When a Cl-containing fuel is used in a CLC process, the potential reactions between Fe-based OCs and HCl should be reduced to lessen the consumption of OCs. Generally, Fe_2O_3 is mainly reduced to Fe_3O_4 in the CLC process [32]. Hence, the potential reactions for Fe_xO_y (Fe_2O_3 and Fe_3O_4) and three adsorbents (CaO, K_2O and Na_2O) with HCl in the FR were analyzed in Fig. 3(a). In addition, the reactions between corresponding chloride and O_2 in the AR are presented in Fig. 3(b).

As shown in Fig. 3 (a), the $\triangle G$ of R1–R2 between 600 and 1000 °C is always greater than zero, implying that the corresponding reaction cannot spontaneously proceed in the positive direction [38]. These results indicate that the two oxidation states of Fe cannot react with HCl in thermodynamics, so HCl can always exist in the CLC process when using raw Fe-based OCs. Additionally, the $\triangle G$ of R3–R5 between 600 and 1000 °C is less than zero, indicating the feasibility of dechlorination for three adsorbents (CaO, K_2O and Na_2O) in thermodynamics. Next, whether these chlorides produced in the FR can react with O_2 in the AR or not requires further examination. If these chlorides can react with O_2 in the AR, then intractable corrosion problems along with undesired secondary pollution occur. Figure 3(b) shows the $\triangle G$ of R6–R8 between 600 and 1000 °C. All three reactions (R6–R8) have values of $\triangle G$ greater than zero, that is, these reactions are not thermodynamically feasible. This result indicates that the three chlorides that are produced in the FR cannot react with O_2 in the AR. Overall, these chlorides, which come from adsorbents reacting with HCl, can, in theory, be accumulated on the surface of the oxygen carrier.

3. Experimental

3.1. Materials

A medical perfusion tube is a typical form of plastic waste that contains abundant chlorine components (such as polyvinyl chloride) [5]. The medical perfusion tube sample was provided by the Health Center of Huazhong University of Science and Technology (HUST) and used as the fuel in this work. The sample was first dried in an oven at 105 °C for 24 h. Next, it was milled and sieved to obtain symmetrical particles from 0.1 mm to 0.2 mm. The elemental composition, proximate analysis and calorific value of the sample are listed in Table 1. The proximate analysis was conducted following the ASTM D5373 criterion. In addition, the ultimate analysis was conducted using an elemental analyzer through the GB212-91/GB212-84 criterion. The contents of C_{ad}, H_{ad}, N_{ad} and S_{ad} were directly determined, while the Cl_{ad} content was measured using an ion chromatograph (ICS-90) as follows: first, 0.2 g of medical plastic was placed within a furnace, and then, the furnace was heated to 1100 °C at 10 °C/min under air atmosphere. Next, the exhaust gas from the reactor was led into the

Table 1
Data from the elemental composition, proximate analysis and calorific value of medical plastics.

Sample	Proximate analysis (wt%)				Ultimate analysis (wt%)					Calorific value (MJ kg^{-1})
	M_{ad}	FC_{ad}	V_{ad}	A_{ad}	C_{ad}	H_{ad}	N_{ad}	S_{ad}	Cl_{ad}	
Medical plastics	0.03	0.08	93.79	6.1	73.89	10.82	0.72	0.16	4.92	33.87

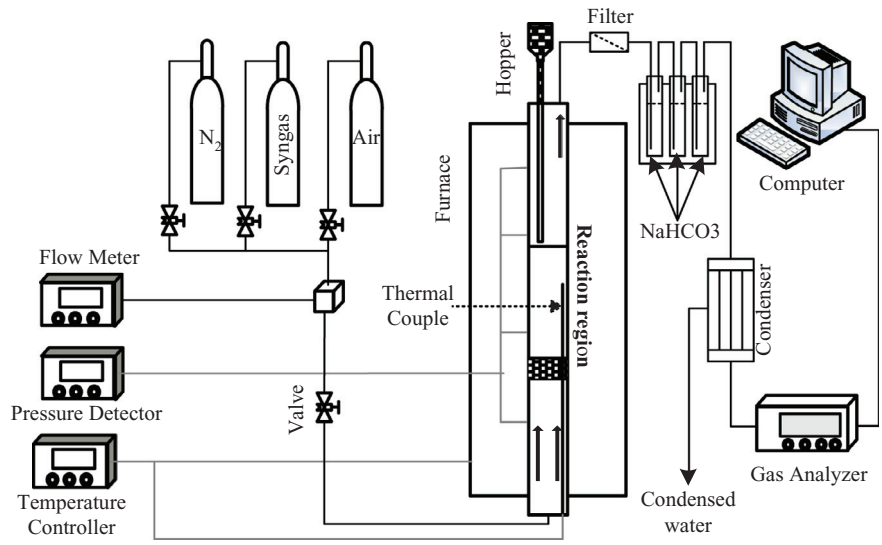

Fig. 4. Overview of the fluidized-bed reactor.

$NaHCO_3$ saturated solution, where Cl_{ad} was measured by detecting the chloride ion concentration.

The OCs consisting of 60 wt% Fe_2O_3 and 40 wt% Al_2O_3 were manufactured using the co-precipitation method. The process is as follows. First, 909 g of $Fe(NO_3)_3 \cdot 9H_2O$ (ACS reagent, purity > 98.5 wt%) and 882.35 g of $Al(NO_3)_3 \cdot 9H_2O$ (ACS reagent, purity > 98.5 wt%) were dissolved in 3 L of deionized water. Second, the aqueous solutions were stirred constantly at 600 rpm, and precipitation isothermally occurred at 363 K and atmospheric pressure, and the pH of the slurry were controlled within 9.0–10.0 by adding ammonium hydroxide. Next, these precursors were dried at 358 K in air for 24 h. Last, these resultant colloidal precursors were calcined at 1273 K for 6 h and then sieved to a size range 0.2–0.3 mm for the subsequent experiments.

Three adsorbents (K_2O, Na_2O and CaO) were added to the raw Fe-based OC particles using the wet impregnation method [39]. The similar process was as follows. First, KNO_3, $NaNO_3$, and $Ca(NO_3)_2 \cdot 4H_2O$ (purity > 99.0 wt%; size < 5 μm) were dissolved in deionized water, and then, an approximately 100-mL salt solution was obtained. Next, the prepared raw Fe-based OC particles described above were soaked in this solution. Subsequently, the mixture was stirred for 12 h at ambient temperature and then dried in the air at 105 °C, followed by these precursors being calcined at 1100 °C for 3 h. Eventually, these nitrates turned into the corresponding metal oxide, and finally, practicable particles (0.2–0.3 mm) were yielded.The mass ratio of adsorbent to OC particles (adsorbent/OC particles) was controlled during the wet impregnation process. Three mass ratios of CaO to OC of 5 wt%, 10 wt%, and 15 wt%, were chosen, while only one mass ratio of N_2O or K_2O to OC of 5 wt% was specified.

To examine the effect of the decoration method, the Fe_2O_3/Al_2O_3 OC particles were doped with CaO by three different methods (wet impregnation, coprecipitation and physical mixture), and the mass ratio of the CaO to OC particles was 5 wt%. For the coprecipitation method, $Ca(NO_3)_2 \cdot 4H_2O$ was added to aqueous solutions during the co-precipitation process. For the physical mixture method, 0.2–0.3 mm CaO particles were directly mixed with Fe-based OCs.

The gaseous fuel was synthesized as 5.9 vol% CH_4, 21.9 vol% CO, 7.8 vol% CO_2, 12.7 vol% H_2, 1 vol% HCl and 50.7 vol% N_2. The gas components mainly relied on the pyrolysis result of medical plastics presented in Section 4.1.

3.2. Apparatus and procedure

The pyrolysis experiments of the medical plastics and the dechlorination experiments were conducted in a laboratory-scale fluidized bed. An overview of the fluidized-bed system is presented in Fig. 4. The system consisted of a gas feeding unit, a fluidized-bed reaction unit, a filter, an $NaHCO_3$ aqueous solution, an electric condenser and a gas analyzer (Gasboard-3151). A straight stainless steel tube (i.d. = 26 mm, length = 892 mm) with a porous distributor plate located 400 mm from the bottom was used as the reaction chamber. The reaction chamber was electrically heated by a furnace. A detailed description of this system can be found elsewhere [40–43]. For the pyrolysis experiments of medical plastics, 30 g of silica sand was placed within the reactor, and then, the furnace was heated to 900 °C. Nitrogen stream (600 mL/min) was introduced into the reactor. After the furnace temperature was stabilized at the set-point temperature, 0.2 g of medical plastics was introduced into the furnace. The concentrations of CO_2, CO, CH_4, H_2, and O_2 were measured using on-line gas analyzers, while the concentration of HCl was measured using an ion chromatograph.

To determine the fundamental reduction kinetics between raw Fe_2O_3/Al_2O_3 or adsorbent-decorated Fe_2O_3/Al_2O_3 OCs and synthesis gas, isothermal kinetic experiments were carried out in a thermogravimentric analyzer (WCT-1D). The schematic of TGA is shown in Fig. 5. Weight variation, as a function of time, was monitored throughout the reduction experiments, which were carried out isothermally. The microbalance of the TGA apparatus has a nominal sensitivity of 0.1 μg. A sample of approximately 20 mg was heated in air in a plate crucible made of Al_2O_3 to the desired reaction temperature (850–925 °C) and then maintained 30 min to ensure sufficient

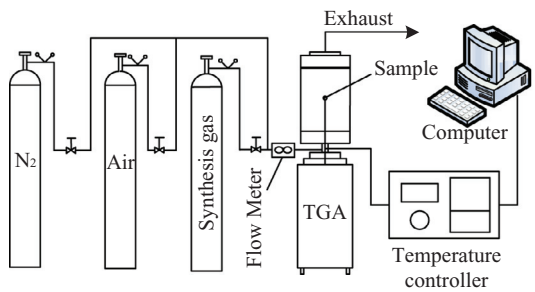

Fig. 5. Schematic of TGA experiments.

oxidation of OC particles. As noted earlier, a HCl-containing synthesis gas was introduced during the reduction reaction of OC particles. To avoid the mixing of reduction gases and air, the system was flushed with N_2 for 10 min before each reduction reaction. The gas flow into the TGA was controlled using an electronic mass flow regulator and all gas flow rates were 40 mL/min. In the experiments, the reduction time was 5 min. The reduction kinetics was then determined by monitoring the weight change of the sample during its reduction.

For the batch fluidized bed dechlorination experiments of each OC sample, a batch of 30 g of OC particles was placed within the reactor, and then, the reactor was heated in an air atmosphere to the set-point temperatures. After the heating was maintained for 10 min, the inlet gas was switched to N_2 for approximately 5 min. When the O_2 concentration of the flue gas became nearly zero, the synthesis gas was introduced to the reactor for approximately 144 s, ensuring that Fe_2O_3 was reduced to Fe_3O_4. When the synthesis gas was oxidized, the inlet gas was switched to N_2 for approximately 5 min to initiate another redox cycle. In these experiments, the flows of N_2, synthesis gas and air were 600 mL/min. After these experiments, the morphologies and surface composition of OC particles were examined using an Environmental Scanning Electron Microscope coupled with an Energy Dispersive X-Ray spectroscopy system (ESEM-EDX, FEI Quanta 2000).

3.3. Data evaluation

For pyrolysis and dechlorination experiments, the volume flow rate of inlet N_2 (N_{N_2}) under the standard conditions was constant, and the gas concentrations of the outlet gases (X_i, $i = CO_2$, CO, CH_4, and H_2) were analyzed by the gas analyzer. $N_{i,\text{out}}$ is defined as the volume flow rate of gaseous product species i, which can be calculated via the N_2 balance [6].

$$N_{i,\text{out}} = \frac{N_{N_2}}{1 - \sum_i X_i} X_i \tag{5}$$

The cumulative volume of gas i ($V_{i,\text{out}}$) was calculated as:

$$V_{i,\text{out}} = \int_0^{t_1} N_{i,\text{out}} dt \tag{6}$$

where t_1 is the duration of the monitoring outlet gases (X_i, $i = CO_2$, CO, CH_4, and H_2).

The degree of conversion for reduction in TGA is defined as:

$$X = \frac{m_0 - m(t)}{m_0 - m_f} \tag{7}$$

where $m(t)$ is the instantaneous weight of the solid during the exposure to HCl-containing synthesis gas. Parameters m_0 and m_f are initial and final weights of the OC particles, respectively. In this study, the initial weight was considered as the weight of OC particles at oxidation stateand the final weight as the weight of OC particles at reduction state when Fe_2O_3 was all converted to Fe_3O_4.

In the batch fluidized bed dechlorination experiments, the dechlorination efficiency, η, was calculated as:

$$\eta = \left(1 - \frac{n_i}{n_0}\right) \times 100\% \tag{8}$$

where n_0 is the total molar content of chlorine in synthesis gas during different redox processes; n_i is the total chlorine molar content in the $NaHCO_3$ solution (which was used for HCl collection for the flue gas) during the corresponding redox processes, which can be detected using an ion chromatograph (ICS-90).

Both the combustible components in the reduction period (FR) and the CO_2 in the oxidation period (AR) were measured using a gas analyzer (Gasboard-3151). The combustion efficiency, φ, which represented the combustion degree of synthesis gas and also acts a measurement for the OC reactivity and CLC performance, was defined as the fraction of introduced fuel that was fully converted into CO_2 and H_2O in the entire reduction period.

$$\phi = \left(1 - \frac{0.5V_{\text{CO,out,FR}} + 0.5V_{\text{H}_2\text{,out,FR}} + 2V_{\text{CH}_4\text{,out,FR}} + V_{\text{CO}_2\text{,out,AR}}}{0.5V_{\text{CO,in,FR}} + 0.5V_{\text{H}_2\text{,in,FR}} + 2V_{\text{CH}_4\text{,in,FR}}}\right) \times 100\% \tag{9}$$

where $V_{\text{CO,in,FR}}$, $V_{\text{H}_2\text{,in,FR}}$ and $V_{\text{CH}_4\text{,in,FR}}$are the volumes of combustible gas that flow into the FR. Similarly, $V_{\text{CO,out,FR}}$,$V_{\text{H}_2\text{,out,FR}}$ and $V_{\text{CH}_4\text{,out,FR}}$ are the volumes of combustible gas that flow out from the FR, and $V_{\text{CO}_2\text{,out,AR}}$ is the volume of carbonaceous gas that flows out from the AR.

4. Results and discussion

4.1. Pyrolysis components of medical waste

The main pyrolysis products (CO_2, CO, CH_4 and H_2) of medical plastic at 900 °C were detected using an on-line gas analyzer. Additionally, the volume of HCl was calculated based on the test results of ion chromatography. The volume flow rate and volume of these pyrolysis products were calculated according to Eqs. 5 and 6, as shown in Fig. 6. Figure 6(a) shows that the main pyrolysis time-period was within the first 100 s. The amount of CO was the largest, which represents 44.4 vol% of the five components. In addition, the percentages of CH_4, CO_2, H_2 and HCl were approximately 12.1 vol%, 15.8 vol%, 25.8 vol% and 1.9 vol%, respectively. The proportion of these five components provided the reference for composing the synthesis gas used in the following experiments.

4.2. Reduction kinetics

Only the transformation from hematite to magnetite ($Fe_2O_3 \rightarrow Fe_3O_4$) may be applicable for industrial CLC systems [44], so the kinetics of first reduction stage ($Fe_2O_3 \rightarrow Fe_3O_4$) was studied in this work.The conversions for reduction profiles of raw Fe_2O_3/Al_2O_3, CaO-decorated Fe_2O_3/Al_2O_3, K_2O-decorated Fe_2O_3/Al_2O_3 and Na_2O-decorated Fe_2O_3/Al_2O_3 with HCl-containing synthesis gas during the reduction processes at different temperatures ($T = 850$, 875, 900 and 925 °C) are shown in Fig. 7. As seen in Fig. 7 (a), a larger conversion for reduction can be found for a higher temperature within the same reduction time period, which means that a higher temperature favors the gas-solid reaction. As presented in Fig 7 (b–(d), the weight loss curves of adsorbent-decorated Fe_2O_3/Al_2O_3 are similar to these of raw Fe_2O_3/Al_2O_3 at 850, 875, 900 and 925 °C. Moreover, note that three adsorbent decorations all delay the end time of the first reduction stage ($Fe_2O_3 \rightarrow Fe_3O_4$). A possible explanation for it is that the adsorbent decoration hinders the transfer of active lattice oxygen in OC particles.

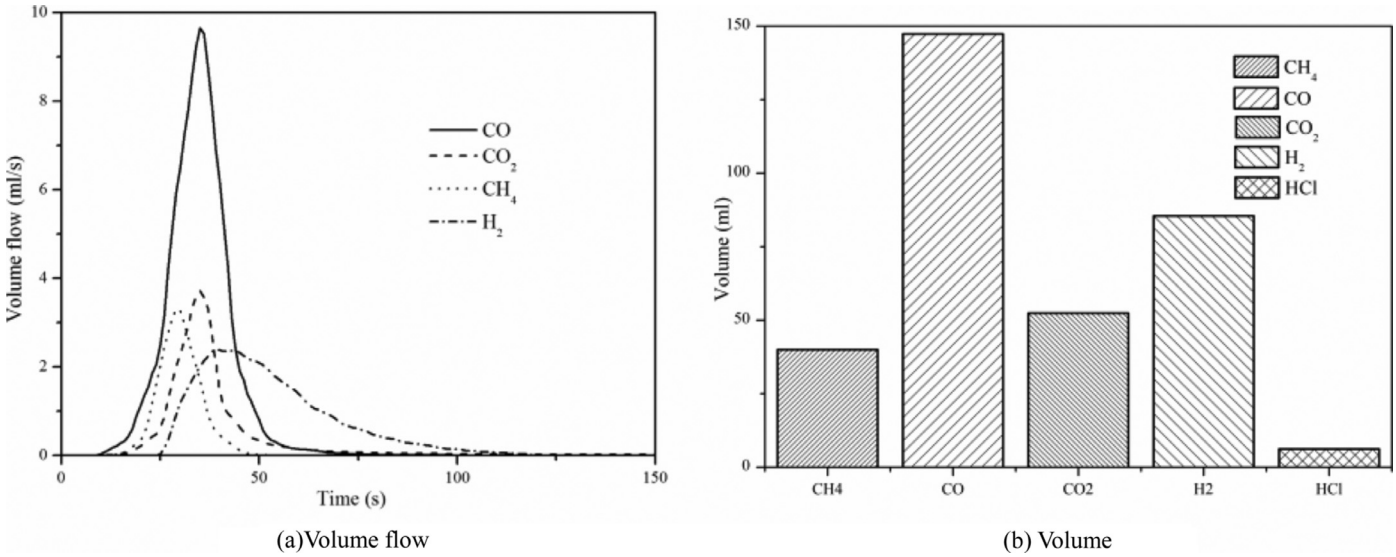

Fig. 6. Volume flow rate and volume of the main pyrolysis components of medical plastics at 900 °C.

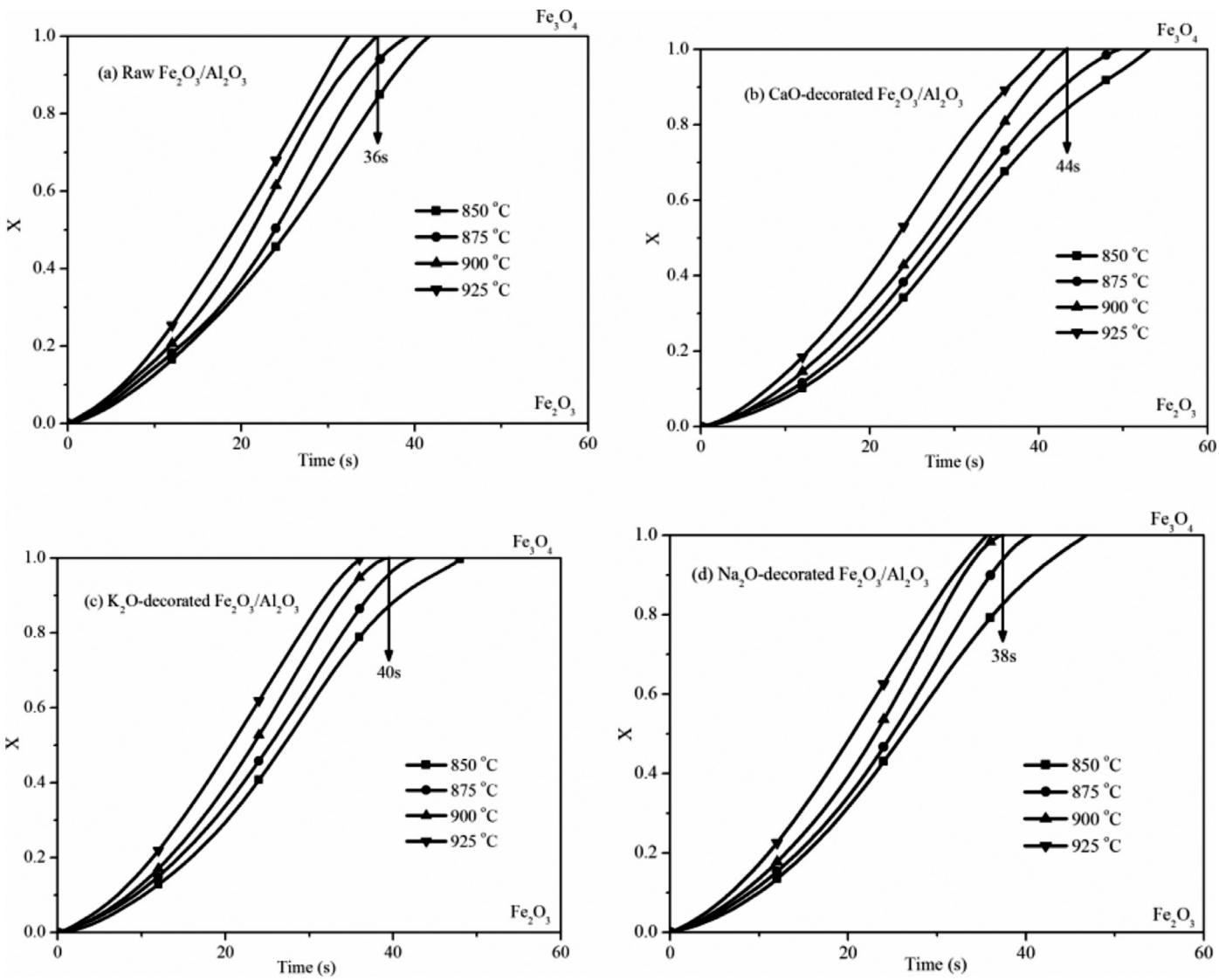

Fig. 7. TGA weight loss profiles obtained from reduction of (a) raw Fe_2O_3/Al_2O_3 (b) CaO-decorated Fe_2O_3/Al_2O_3, (c) K_2O-decorated Fe_2O_3/Al_2O_3 and (d) Na_2O-decorated Fe_2O_3/Al_2O_3 at different temperatures when using HCl-containing synthesis gas as fuel.

Table 2
Kinetic equations for different reaction mechanisms.

Reaction mechanism	Integral form $G(X)=kt$
1-D diffusion	X^2
2-D diffusion	$X+(1-X)\ln(1-X)$
3-D diffusion-Jander	$[1-(1-X)^{1/3}]^2$
Phase boundary-controlled(contracting cylinder)	$1-(1-X)^{1/2}$
Phase boundary-controlled(contracting sphere)	$1-(1-X)^{1/3}$
First order reaction	$-\ln(1-X)$
2-D growth of nuclei	$[-\ln(1-X)]^{1/2}$
3-D growth of nuclei	$[-\ln(1-X)]^{1/3}$

Kinetic parameters can be obtained from these isothermal kinetic data using the rate law equation,

$$\frac{dX}{dt} = kf(X) \tag{10}$$

$$k = Ae^{-E/RT} \tag{11}$$

Integrating Eq. (11) gives

$$\int_0^X \frac{dX}{f(X)} = G(X) = kt \tag{12}$$

where X is the factional conversion, t is time, k is the reaction rate constant, A is the pre-exponential factor, E is the activation energy, R is gas constant, T is absolute temperature, and $f(X)$ and $G(X)$ are the differential form and integral form expressions for the reaction mechanism [44].

The rate constant k can be determined by applying Eq. (12). The values of $G(X)$ are first plotted with time t and then fitted by a straight line with the intercept equal to zero. Note that by taking the logarithm of Eq. (11) we have

$$\ln k = \ln A + \left(-\frac{E}{R}\right)\frac{1}{T} \tag{13}$$

The relation of the k values with the reaction temperature is then established by the Arrhenius plots. It results in a straight line with the slope of $-E/R$ and an intercept that is the logarithm of pre-exponential factor A.

Three groups of kinetic models were normally used to interpret the reaction mechanism for solid-gas reactions. These are (a) diffusion-controlled models, (b) phase boundary-controlled models, and (c) nucleation and growth models. A variety of algebraic equations were derived to illustrate these models in a mathematical manner with relevant assumptions. The equations presented in Table 2 are typically used for modeling the kinetic data of solid-gas reactions mathematically [44].

To determine the optimum kinetic model for these experimental data, all of eight mechanism models were applied for the reduction result of raw Fe_2O_3/Al_2O_3 at 900 °C, as shown in Fig. 8. Based on Eq. (12), the value of $G(X)$ should be a linear relationship with t. It can be seen that the 3-D nuclei growth model can conform to the requirement. Subsequently, the rate constant k and the correlation coefficient (R^2) of all reduction processes were calculated, as

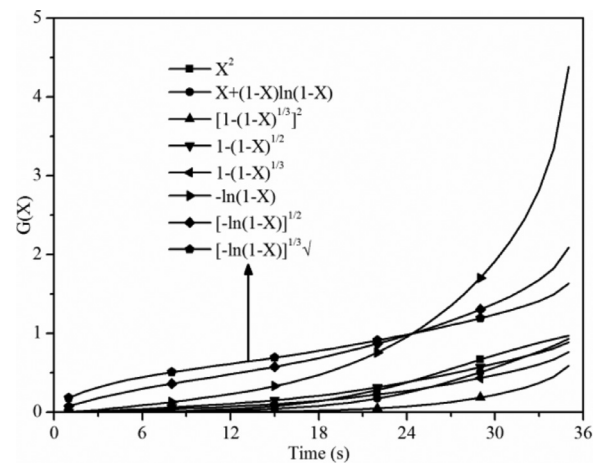

Fig. 8. Integral form expressions of eight reaction mechanisms for raw Fe_2O_3/Al_2O_3 reacting with HCl-containing synthesis gas at 900 °C

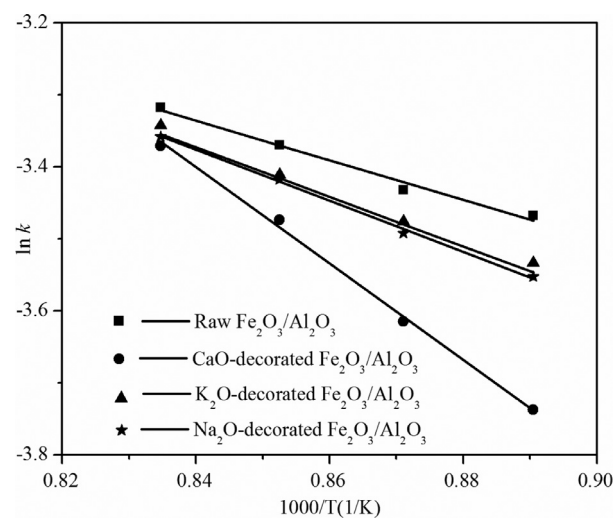

Fig. 9. Plots of ln k vs. 1000/T for the reduction of four OCs with HCl-containing synthesis gas.

shown in Table 3. Note that the least correlation coefficients are not less than 0.97592, which demonstrates the reliability of 3-D nuclei growth model.

As the above mentioned, the linear regression analysis of the experimental data of ln k vs. 1000/T was used to determine E/R. Plots of ln k versus 1000/T are shown in Fig. 9 for different OC particles. As expected, they are straight lines with negative slopes, which are then used to estimate the kinetic parameters. The obtained activation energy and pre-exponential factor are listed in Table 4. It is found that the activation energy of raw Fe_2O_3/Al_2O_3 is 22.82 kJ/mol and less than that of others, which indicates that the raw Fe_2O_3/Al_2O_3 is much easier to be reduced by HCl-containing synthesis gas. Adsorbent decoration results in the increase of activation energy, especially for CaO

Table 3
Reduction kinetic study of four OC particles.

Temperature (°C)	Raw Fe_2O_3/Al_2O_3		CaO-decorated Fe_2O_3/Al_2O_3		K_2O-decorated Fe_2O_3/Al_2O_3		Na_2O-decorated Fe_2O_3/Al_2O_3	
	k	R^2	k	R^2	k	R^2	k	R^2
850	0.03118	0.98459	0.02381	0.99781	0.02919	0.99382	0.02865	0.99013
875	0.03232	0.97719	0.02692	0.98981	0.03093	0.98096	0.03043	0.98203
900	0.03438	0.97746	0.03101	0.98852	0.03301	0.9842	0.03279	0.97592
925	0.03622	0.98996	0.03436	0.99326	0.03534	0.98753	0.03481	0.9828

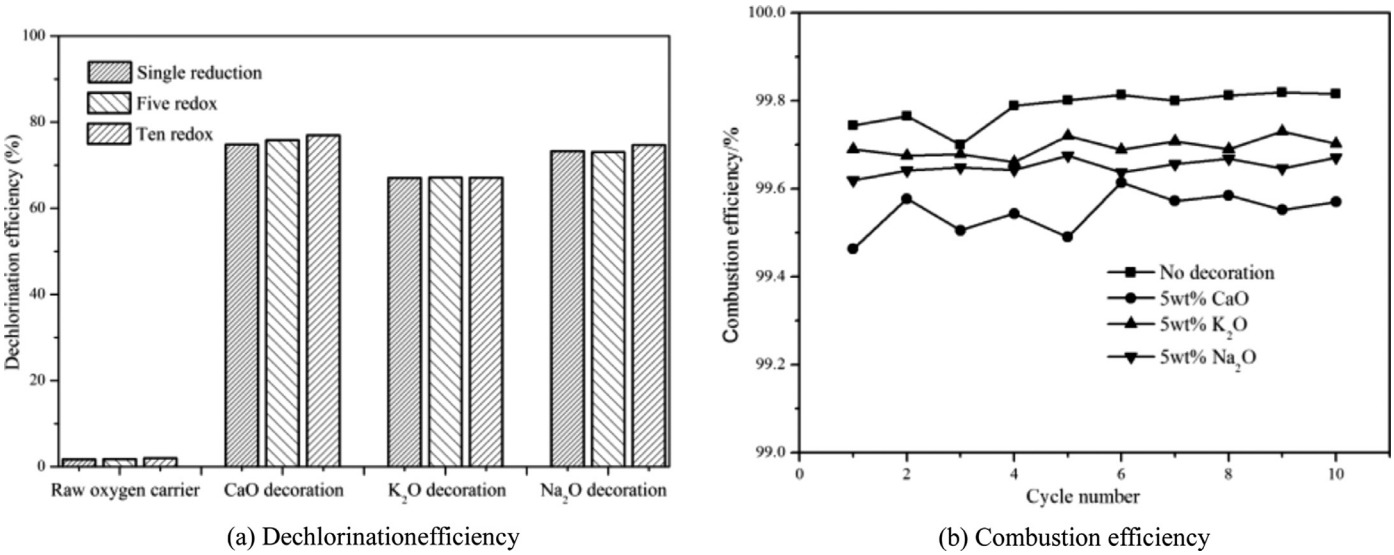

Fig. 10. Dechlorination and combustion efficiencies for different OC particles at 900 °C.

Table 4
Kinetic parameters of reduction for different OCs with synthesis gas between 850 °C and 925 °C.

Sample	E(kJ/mol)	A
Raw Fe_2O_3/Al_2O_3	22.82	0.35669
CaO-decorated Fe_2O_3/Al_2O_3	55.59	9.16984
K_2O-decorated Fe_2O_3/Al_2O_3	28.63	0.61821
Na_2O-decorated Fe_2O_3/Al_2O_3	29.45	0.66928

decoration, which indicates that the adsorbent decoration can lower the reactivity of OC particles to a certain extent.

4.3. Effect of adsorbent species on dechlorination and the combustion efficiency

Raw OC particles and the particles decorated with 5 wt% CaO, K_2O and Na_2O were tested in terms of dechlorination and the combustion efficiency, as shown in Fig. 10. The exhaust gas components for the four groups of fluidized bed experiments are shown in Fig. 11.

When Fe-based OC particles without decoration were used, the dechlorination efficiency was approximately zero. This result indicated that the reaction of Fe_2O_3 with HCl is nearly impossible, which is consistent with the thermodynamic result of Fig. 3(a). For three adsorbent-decorated OCs, the dechlorination efficiencies were 74.78%, 67.07% and 73.27% for CaO decoration, K_2O decoration and Na_2O decoration, respectively. Among these OCs, CaO-decorated OC presented the best dechlorination effect, although the differences among them are not very evident. Generally, the experimental results are consistent with thermodynamic simulation and isothermal kinetic experiments. However, we note that the dechlorination efficiency for the three OCs is negatively related with the Gibbs free energy (absolute value) and the activation energy obtained by the 3-D nuclei growth model. We believe that the dechlorination efficiency of adsorbent-decorated OCs is closely dependent on the intrinsic reactivity of adsorbent with HCl but also the mass and heat transfer under the atmosphere of fluidized bed reactor and physical properties such as surface area and pore structure when these adsorbents were decorated to Fe_2O_3/Al_2O_3 OC particles. In addition, no obvious difference in dechlorination was found in Fig. 10(a) for any type of adsorbent-decorated OC particles undergoing a single reduction, five redox cycles, or ten redox cycles, illustrating that no Cl_2 was released during the oxidation period and the chloride produced in the FR cannot

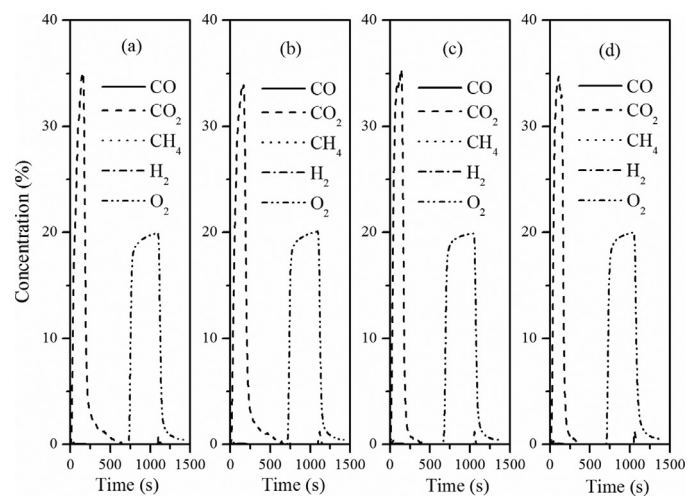

Fig. 11. Gas components with Fe-based OC particles (a) without decoration, (b) with 5 wt% CaO decoration, (c) with 5 wt% K_2O decoration, and (d) with 5 wt% Na_2O decoration.

be oxidized by O_2 in the AR. Furthermore, three types of adsorbent-decorated OCs also demonstrated the favorable stability of dechlorination and reactivity during ten successive redox cycles.

As shown in Fig. 10(b), the decoration of any adsorbent led to a slight decrease in the combustion efficiency. In fact, a minor amount of carbon was deposited onto the surface of OC particles during the reduction period and then burnt out in the AR, resulting in incomplete combustion in the FR. Clearly, the combustion efficiency was negatively related with the dechlorination efficiency. First, this finding should be related with the diffusion limitations in these batch experiments. Another possible explanation for this behavior was that adsorbent decoration hindered the transfer of the active lattice oxygen, leading to a small amount of Fe or FeO generation (which is thermodynamically favorable compared to the carbon formation) [45]. Figure 11 shows the typical gas concentration profiles during a redox process. For these experiments, when the O_2 concentration was decreased to approximately zero, the synthesis gas was introduced into the reactor. Next, the CO_2 concentration sharply increases to approximately 35%, which illustrated the reliable reactivity of Fe-based OC particles. When the synthesis gas was stopped, the CO_2 concentration

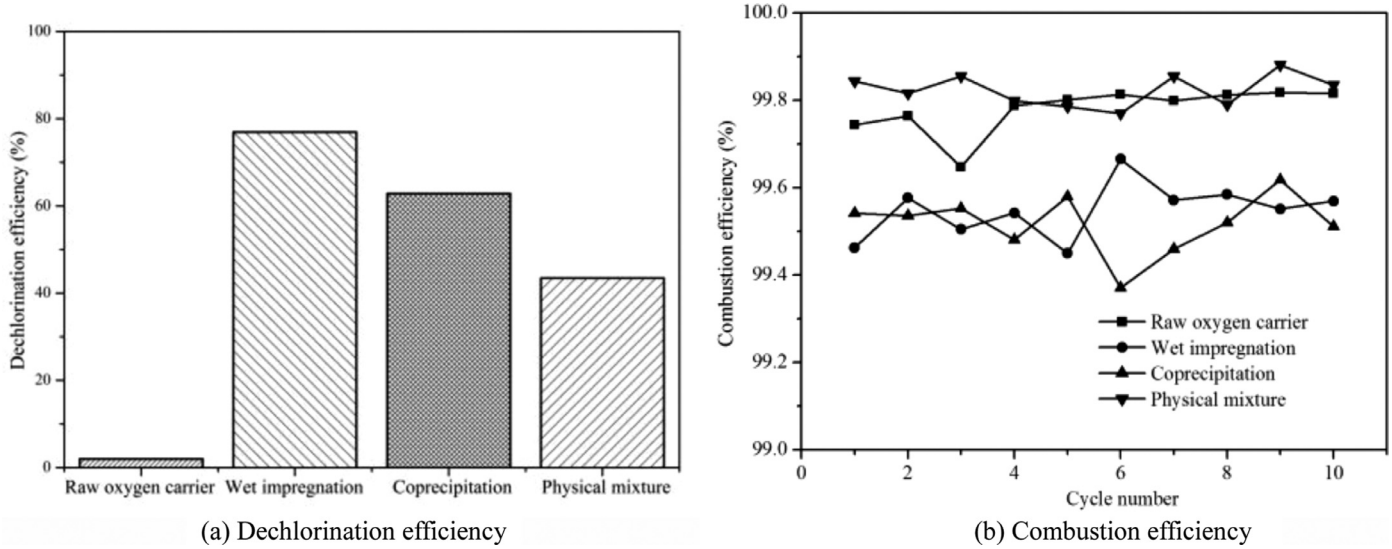

Fig. 12. Efficiencies of dechlorination and combustion for different OC particles at 900 °C.

sharply decreased to approximately 3% and then slowly decreased to zero. As shown in Fig. 11(a)–(d), a small amount of CO_2 was produced in the oxidation periods, although the CO_2 concentration did not exceed 2%. As mentioned above, the small amount of CO_2 originated from the combustion of carbon residue from methane decomposition [46]. Compared with raw OC particles, slightly more carbon deposition occurred after being decorated by any adsorbent. A higher combustion efficiency is expected to be attained if more OC particles are used (stoichiometric OC particles were used in this study).

The introduction of alkali metal oxides (Na_2O, K_2O) into OCs can benefit dechlorination, however will produce alkali chlorides. It is well-known that these alkali chlorides (like NaCl and KCl) would be some tremendously problematic in combustion systems, such as a lower reactivity of adsorbent-decorated OC particles, slagging and fouling. It is fortunate to find that the CaO-decorated OC particles demonstrated the best dechlorination efficiency. Note that CaO adsorbent has been considered as a cheap material and has been widely applied for desulfuration during coal combustion. In this study, the CaO adsorbent, rather than K_2O and Na_2O, is preferred.

4.4. Effect of the decoration method on the efficiencies of dechlorination and combustion

Figure 12 shows the efficiencies of dechlorination and combustion of raw and CaO-decorated OC particles using three decoration methods. For the three CaO-decorated OCs, the dechlorination efficiencies were 76.95%, 62.85% and 43.43% for the wet impregnation method, coprecipitation method and physical mixture method, respectively. Among these OCs, CaO-decorated OC via the wet impregnation method presented the best dechlorination effect. To quantitatively investigate the effect of CaO decoration by different methods on the reactivity of OC particles, the combustion efficiency was calculated, and ten successive redox cycles of CLC with different OC particles were performed, as shown in Fig. 12(b). For the wet impregnation method, CaO decoration led to a slight decrease in the combustion efficiency, which was similar to the result of the coprecipitation method, while the physical mixture method exhibited a much higher combustion efficiency, which was close to that of the raw OC situation. As mentioned above, the CaO partly hindering the contact of OC particles with the synthesis gas may be the possible reason for this higher efficiency. Overall, the wet impregnation method for CaO decoration was considered to be the best choice for dechlorination and also exhibited an acceptable combustion efficiency.

4.5. Effect of CaO loading on the efficiencies of dechlorination and combustion

The CaO loading content is one of main factors that not only can affect the efficiencies of dechlorination and combustion but also can determine the life time of adsorbent-decorated OCs. Raw OC particles and those decorated by 5 wt%, 10 wt% and 15 wt% CaO were tested in the batch fluidized bed reactor. As shown in Fig. 13(a), the difference in dechlorination for the three CaO loading contents was small. One possible reason for this response is that the 5 wt% CaO content was far beyond the requirements for 10 cycles (according to HCl mole amount, it can withstand 80 cycles). Figure 13(b) shows the combustion efficiencies for raw OC particles and those decorated by the three CaO loadings. Similarly, three different CaO loadings for OC particles all led to a slight decrease in the combustion efficiency, while the difference was negligible. Generally, a higher CaO loading content can absorb more CO_2 (which can promote the combustion of CH_4 and CO) and partly hinder the contact of OC particles and synthesis gas, which can explain the slight differences of the three CaO loadings in combustion efficiency. In summary, different CaO loading contents cause an insignificant difference in the efficiencies of dechlorination and combustion. The 5 wt% CaO loading can be considered to be the best for CaO decoration.

4.6. Effect of the reaction temperature on the efficiencies of dechlorination and combustion

Four reaction temperatures, 850 °C, 875 °C, 900 °C and 925 °C, were chosen to investigate the effect of temperature on the efficiencies of dechlorination and combustion using a 5 wt% CaO-decorated Fe_2O_3/Al_2O_3 composite as the OC particles. Figure 14(a) shows that the dechlorination efficiency is improved as the temperature increases and that it can reach 80% at 925 °C. A higher temperature is generally acknowledged to accelerate the gas-solid reaction (between HCl and CaO) [47], which can be deemed to be the main reason for the improved efficiency. However, a higher temperature favors the decomposition of methane [46], which results in the deposition of more carbon. Additionally, these carbon residues are difficult to be oxidized by oxygen carrier particles under an oxygen-deficient atmosphere [48], leading to a decreasing combustion efficiency, as shown

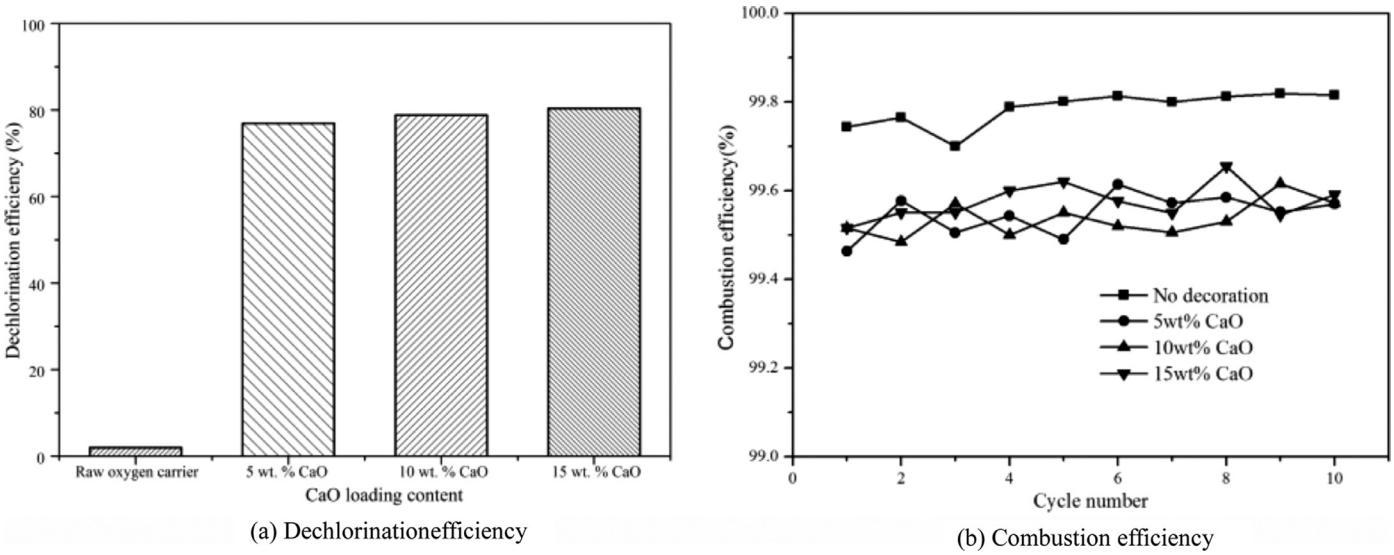

Fig. 13. Efficiencies of the dechlorination and combustion of CaO decoration with different decorated ratios.

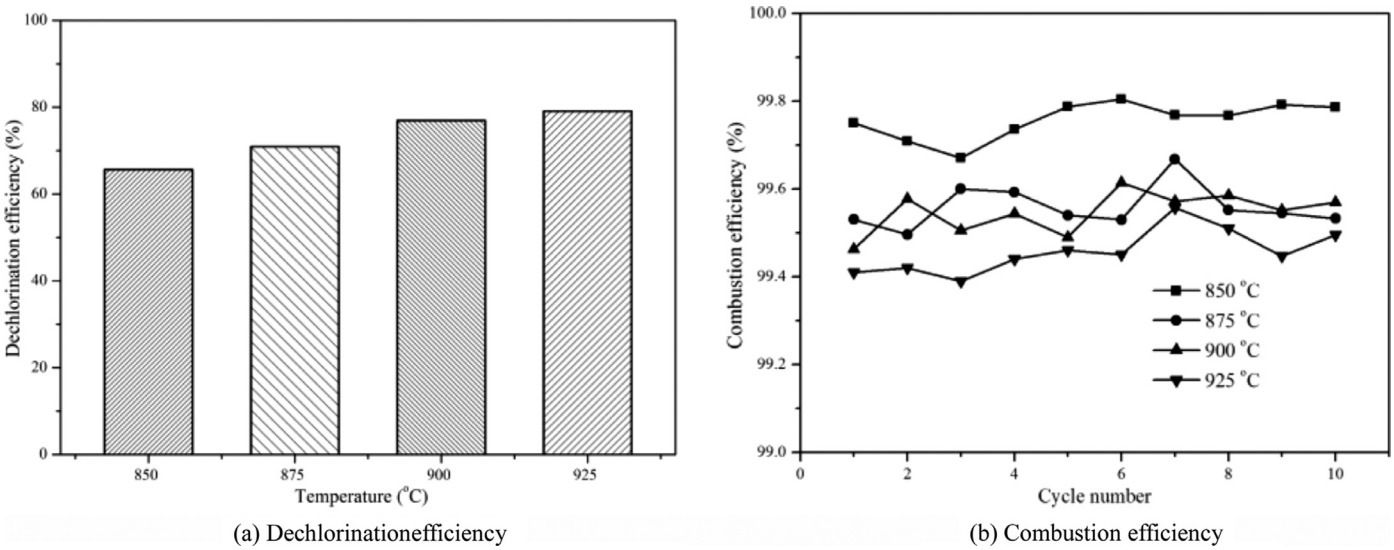

Fig. 14. Efficiencies of the dechlorination and combustion of CaO-decorated Fe_2O_3/Al_2O_3 OC particles at different temperatures.

in Fig. 14(b). Still, we argue that this problem can be overcome if a sufficient number of OC particles are used.

4.7. Long-term tests

A long-term experiment was conducted at 900 °C using 5 wt% CaO-decorated Fe_2O_3/Al_2O_3 to test the durability of dechlorination. As shown in Fig. 15(a), persistently using OC particles during 60 redox cycles results in the decay of dechlorination. After 30 cycles, the dechlorination efficiency is reduced to 65%, and the decay rate of the dechlorination efficiency increases suddenly after the 30th cycle. The decay in dechlorination efficiency is attributed to a portion of CaO in the OC particles being lost during the redox processes. As a result of the loss of CaO, the combustion efficiency gradually increases with the cycle number, as shown in Fig. 15(b).

4.8. ESEM-EDX characterizations

To evaluate the CaO decoration effect, the reduced samples of raw Fe_2O_3/Al_2O_3 OC after the 10th cycle, fresh CaO-decorated Fe_2O_3/Al_2O_3 OC particles, and reduced samples after the 10th, 30th, 60th cycles were characterized using ESEM-EDX. As shown in Fig. 16 (a) and (c), Fe, Al, C and O were detected in both particles. Among these elements, C was derived from coating the samples with carbon to enhance the sample's electrical conductivity. Chlorine was detected on the surface of CaO-decorated OCs after 10 redox cycles (Fig. 16 (c)), whereas it was not found on the non-decorated OC surface (Fig. 16 (a)). This observation demonstrated that chloride, which comes from the CaO adsorbent reacting with HCl, can be accumulated on the surface of the OC particles, which is consistent with the previous thermodynamic results. As shown in Fig. 16 (b), 5 wt% CaO can attain a uniform decoration of the OC particles. EDX characterization clearly indicates the loss of adsorbents during the long-term tests. The mole ratios of Ca and Fe versus the cycle number were fitted in Fig. 16(f), revealing a linear decay of the Ca/Fe molar ratio from a theoretical value (nearly 9.8 mol%) to 1.6 mol%. The rapid decay of the Ca/Fe ratio can explain the rapid decreases in the dechlorination efficiency (Fig. 16(a)) and a linear increase in the combustion efficiency (Fig. 16(b)) with increasing cycle number.

In addition, the reproducibility of the CaO-decorated Fe_2O_3/Al_2O_3 OC that was used was tested by washing the reduced samples after the 30th cycle with a dilute hydrochloric acid solution. These washed OC particles were characterized by ESEM-EDX, as shown in Fig. 17. The result indicated that the residual CaO adsorbent can be

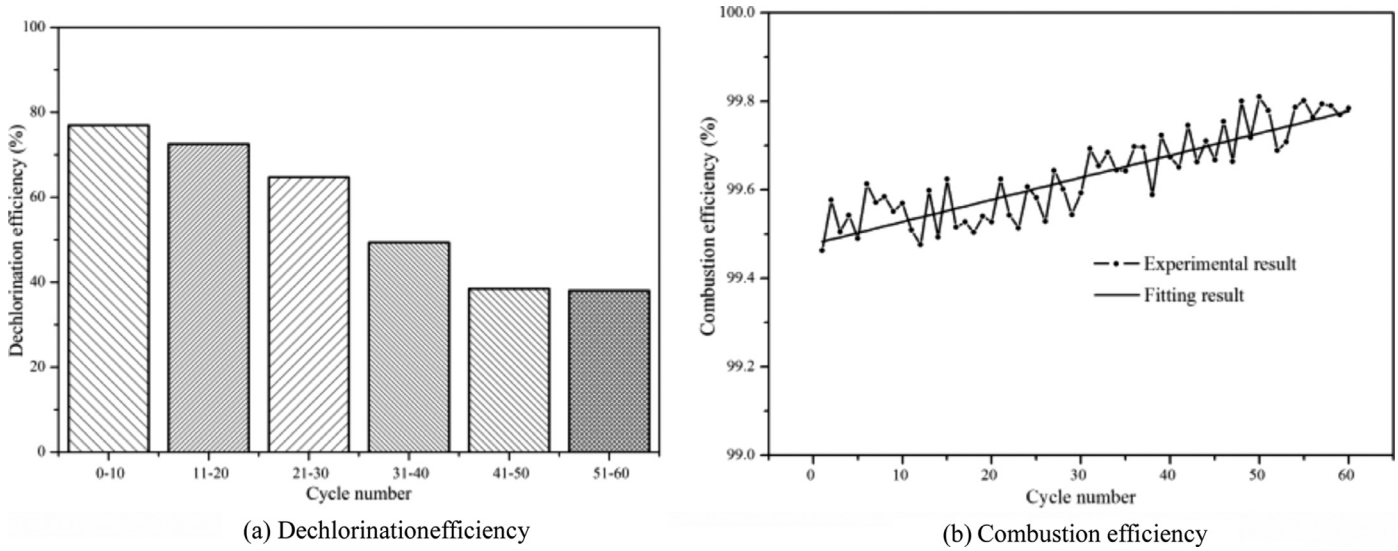

Fig. 15. Efficiencies of the dechlorination and combustion of CaO decoration for 60 cycles.

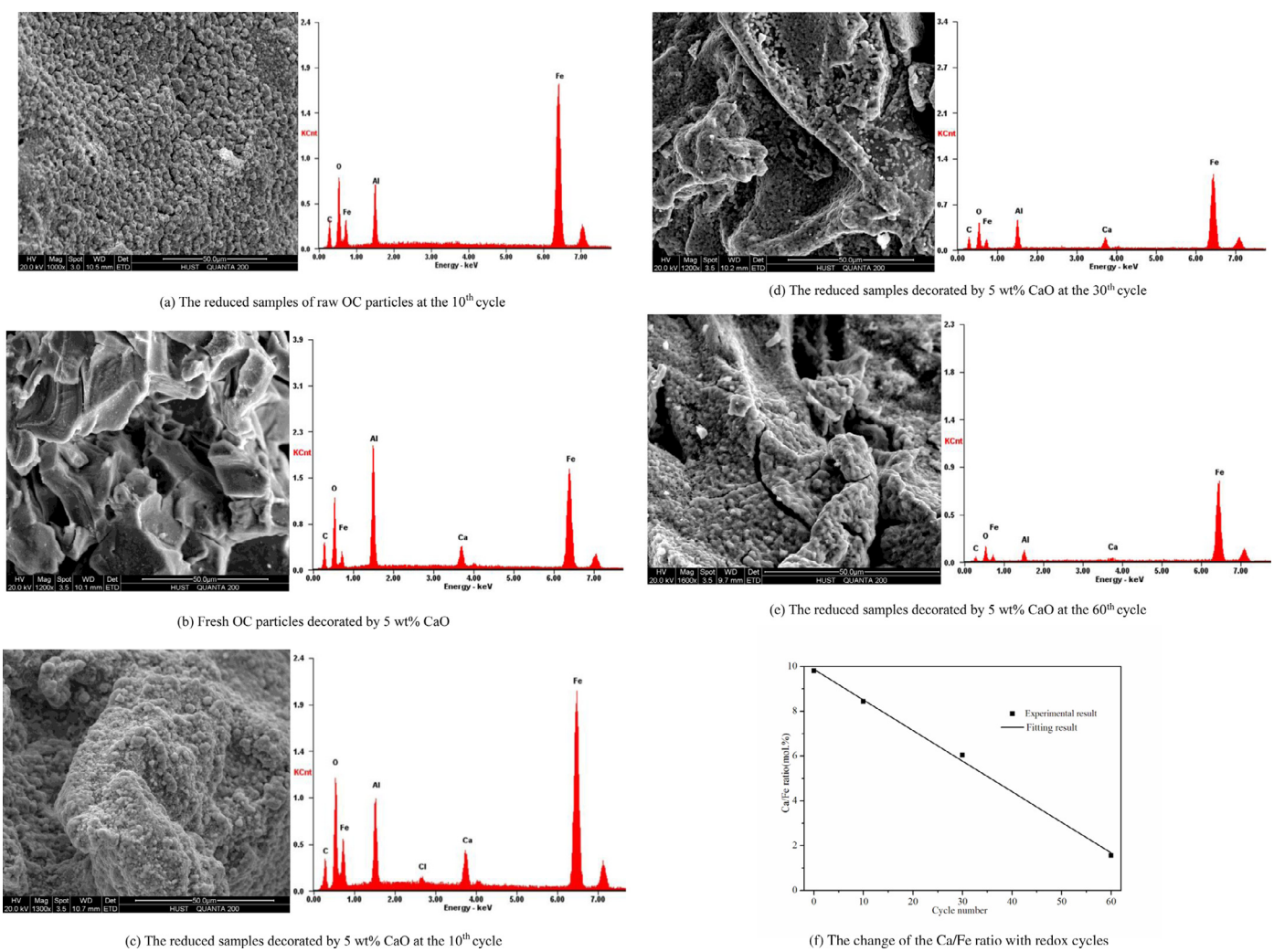

Fig. 16. ESEM images and EDX analysis of different OC particles.

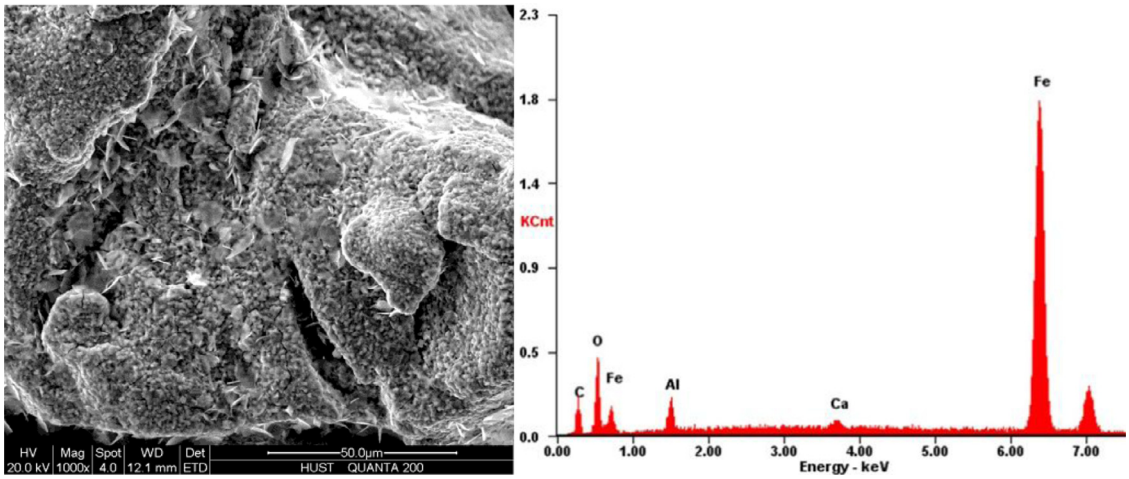

Fig. 17. ESEM images and EDX analysis of the washed OC particles after being used for 30 cycles.

eliminated after washing with a dilute hydrochloric acid solution, which supported the reproducibility of CaO-decorated Fe_2O_3/Al_2O_3 OC particles. Overall, these results demonstrated that dechlorination in chemical looping combustion using CaO decorated Fe-based OCs is feasible. More research studies are required to restrain the decay of the dechlorination efficiency and restrict the adsorbent loss from the OC during long-term tests. Additionally, the CLC of plastic waste and the reduction of the emission of PCDD/Fs from the process are urgently needed.

5. Conclusions

This work, for the first time, utilized adsorbent-decorated Fe_2O_3/Al_2O_3 as OCs for dechlorination during the CLC process. First, the potential reactions of Fe_2O_3 and Fe_3O_4 with HCl, the reactions of three adsorbents (CaO, K_2O and Na_2O) with HCl in the FR, and the reactions of the corresponding chloride with O_2 in the AR were simulated through calculating the Gibbs free energy for a single reaction. The simulation results indicated that HCl hardly interacts with Fe_2O_3 and Fe_3O_4; however, when decorating OCs with these adsorbents, HCl was completely converted into the corresponding chloride in the FR, and these chlorides cannot react with O_2 in the AR. Next, the determined components (5.9 vol% CH_4, 21.9 vol% CO, 7.8 vol% CO_2, 12.7 vol% H_2, 1 vol% HCl and 50.7 vol% N_2) were synthesized as a fuel, and this volume ratio mainly relied on the main pyrolysis products of medical plastics at 900 °C. The reduction kinetics of four OC particles with HCl-containing synthesis was investigated through isothermal TGA experiments. For describing the reduction process of raw Fe_2O_3/Al_2O_3 at 900 °C, eight isothermal kinetic models were applied to determine the most suitable kinetic model. It was found that the translation Fe_2O_3 into Fe_3O_4 can be described by the 3-D nuclei growth model. Then using the 3-D nuclei growth model the apparent activation energy (E) was calculated to be 22.82 kJ/mol, 55.59 kJ/mol, 28.63 kJ/mol and 29.45 kJ/mol for raw Fe_2O_3/Al_2O_3, CaO-decorated Fe_2O_3/Al_2O_3, K_2O-decorated $Fe_2O_3/Al_2O_3$and Na_2O-decorated Fe_2O_3/Al_2O_3, respectively. Subsequently, the effects of adsorbent species (CaO/K_2O/Na_2O), decoration method (wet impregnation, coprecipitation and physical mixture), loading content and temperature on the efficiencies of dechlorination and combustion in chemical looping combustion (CLC) using adsorbent-decorated Fe-based OC were evaluated in a batch fluidized bed reactor, which simulates a real chemical looping process. The experimental results indicated that CaO decoration for OC particles through the wet impregnation method demonstrated the highest dechlorination efficiency, but resulted in more carbon deposition on the OC particles. In addition, 5 wt% CaO can reach optimized dechlorination to ascertain the CaO loading content. Furthermore, increasing the temperature can improve dechlorination at the cost of slightly more carbon deposition, leading to a lower combustion efficiency. Next, by integrating the results of ion chromatography with the results from an environmental scanning electron microscope coupled with energy dispersive X-ray spectroscopy (ESEM-EDX), the dechloridation efficiency was found to gradually decrease; correspondingly, the mole ratio between Ca and Fe on the OC particle surface exhibited a declining trend with the increase of the cycle number. Notably, the ESEM-EDX result also demonstrated the accumulation of Cl elements on the surface of OC particles. Finally, the reduced samples, after thirty cycles, were washed with a dilute hydrochloric acid solution, and the feasibility of removing Ca and Cl from the surface of CaO-decorated OC particles was verified by ESEM-EDX analysis. In summary, these results demonstrated that dechlorination in chemical looping combustion using adsorbent-decorated Fe_2O_3/Al_2O_3 OC particles is feasible.

It is worth noting that during the in-situ gasification chemical looping combustion of plastic waste the HCl would be released and well-mixed, which would lead to different HCl residence times and atmospheres in the FR, and thus would involve the formation of PCDD/Fs. Because the HCl-containing synthesis gas from a pyrolysis experiment of medical plastics at 900 °C was used as fuel for the dechlorination investigation, and the residence time of synthesis gas is generally different from that of pyrolysis products in the iG-CLC of plastic waste, it is difficult to investigate accurately the effect of residence time of HCl and reactor atmosphere in this study. It is deserved to investigate directly the iG-CLC of plastic waste in the next stage. Also, the emission of dioxings/furans in this study would be very little, lower than the measurement limit. The experimental measurement of PCDD/Fs during the continuous iG-CLC processes will be conducted in the next stage.

Acknowledgments

These authors were supported by the National Natural Science of China (51561125001 and 51390494). We are also thankful to anonymous reviewers for their useful comments, which illumined the authors greatly and improved the paper substantially. The authors are grateful to the Analytical and Testing Center of HUST for SEM-EDX measurements.

References

[1] M. Chaerul, A.R. Fahruroji, T. Fujiwara, J. Mater. Cycles Waste Manag. 16 (2014) 509–518.
[2] M. Yan, X.D. Li, S.Y. Lu, T. Chen, Y. Chi, J.H. Yan, J. Mater. Cycles Waste Manag. 13 (2011) 213–218.

[3] J.H. Yan, T. Chen, X.D. Li, J. Zhang, S.Y. Lu, M.J. Ni, K.F. Cen, J. Hazard. Mater. 135 (1–3) (2006) 47–51.
[4] S. Seidelt, M. Müller-Hagedorn, H. Bockhorn, J. Anal. Appl. Pyrol. 75 (1) (2006) 11–18.
[5] S. Singh, C. Wu, P.T. Williams, J. Anal. Appl. Pyrol. 94 (0) (2012) 99–107.
[6] H.M. Zhu, X.G. Jiang, J.H. Yan, Y. Chi, K.F. Cen, J. Anal. Appl. Pyrol. 82 (1) (2008) 1–9.
[7] R. Lu, S. Purushothama, X. Yang, J. Hyatt, W.-P. Pan, J.T. Riley, W.G. Lloyd, Fuel Process. Technol. 59 (1) (1999) 35–50.
[8] A. Hoyos, M. Cobo, B. Aristizábal, F. Córdoba, C.Md. Correa, Chemosphere 73 (1) (2008) S137–S142.
[9] Y. Chen, R. Zhao, J. Xue, J. Li, Waste Manag. 33 (2013) 1165–1173.
[10] H.C. Wang, S.H. Chang, P.C. Hung, J.F. Hwang, M.B. Chang, Chemosphere 71 (2013) 388–397.
[11] E. Weidemann, S. Marklund, H. Bristav, L. Lundin, Chemosphere 102 (2014) 12–17.
[12] H.L. Wu, S.Y. Lu, X.D. Li, X.G. Jiang, J.H. Yan, M.S. Zhou, H. Wang, Chemosphere 86 (2012) 361–367.
[13] L. Lundin, M.F. Gomez-Rico, C. Forsberg, C. Nordenskjöld, S. Jansson, Chemosphere 91 (6) (2013) 797–801.
[14] L. Lundin, S. Jansson, Chemosphere 94 (2014) 20–26.
[15] Y.-F. Wang, L.-C. Wang, L.-T. Hsieh, H.-W. Li, H.-C. Jiang, Y.-S. Lin, C.-H. Tsai, Aerosol Air Qual. Res. 12 (2012) 191–199.
[16] A. López, I. de Marco, B.M. Caballero, M.F. Laresgoiti, A. Adrados, Fuel Process. Technol. 92 (2) (2011) 253–260.
[17] C.J.E. Bajamundi, P. Vainikka, M. Hedman, I.H. nen, J. Silvennoinen, T. Heinanen, R. Taipale, J. Konttinen, Fuel 134 (2014) 677–687.
[18] B.R. Stanmore, Combust. Flame 136 (3) (2004) 398–427.
[19] M. Yan, X.D. Li, T. Chen, S.Y. Lu, J.H. Yan, K.F. Cen, J. Environ. Sci. 22 (2010) 1637–1642.
[20] X. Lin, Q. Huang, T. Chen, X. Li, S. Lu, H. Wu, J. Yan, M. Zhou, H. Wang, Aerosol Air Qual. Res. 14 (2014) 1142–1151.
[21] H.-J. Zhang, Y.-W. Ni, J.-P. Chen, Q. Zhang, Chemosphere 70 (2008) 721–730.
[22] M. Iggland, H. Leion, T. Mattisson, A. Lyngfelt, J. Environ. Sci. 65 (22) (2010) 5841–5851.
[23] H. Leion, A. Lyngfelt, M. Johansson, E. Jerndal, T. Mattisson, Chem. Eng. Res. Des. 86 (9) (2008) 1017–1026.
[24] E. Grandesso, B. Gullett, A. Touati, D. Tabor, Sci. Technol. 45 (2011) 3887–3894.
[25] D. Mei, A. Abad, H. Zhao, J. Adanez, C. Zheng, Energy Fuels 28 (2014) 7043–7052.
[26] M.K. Chandel, A. Hoteit, A. Delebarre, Fuel 88 (5) (2009) 898–908.
[27] P. Gayán, L.F. de Diego, F. García-Labiano, J. Adánez, A. Abad, C. Dueso, Fuel 87 (12) (2008) 2641–2650.
[28] P. Gayán, C. Dueso, A. Abad, J. Adánez, L.F. de Diego, F. García-Labiano, Fuel 88 (6) (2009) 1016–1023.
[29] C. Linderholm, A. Lyngfelt, A. Cuadrat, E. Jerndal, Fuel 102 (2012) 808–822.
[30] L.F. de Diego, F. Garcı´a-Labiano, P. Gayán, J. Celaya, J.M. Palacios, J. Adánez, Fuel 86 (7–8) (2007) 1036–1045.
[31] L.H. Shen, J.H. Wu, Z.P. Gao, J. Xiao, Combust. Flame 157 (5) (2010) 934–942.
[32] L.H. Shen, J.H. Wu, Z.P. Gao, J. Xiao, Combust. Flame 156 (7) (2009) 1377–1385.
[33] E.R. Monazam, R.W. Breault, R. Siriwardane, Energy Fuels 28 (2014) 5406–5414.
[34] H.M. Gu, L.H. Shen, J. Xiao, S.W. Zhang, T. Song, D.Q. Chen, Combust. Flame 159 (7) (2012) 2480–2490.
[35] L.H. Shen, J.H. Wu, J. Xiao, Combust. Flame 156 (3) (2009) 721–728.
[36] R. Xiao, Q. Song, M. Song, Z. Lu, S. Zhang, L. Shen, Combust. Flame 157 (6) (2010) 1140–1153.
[37] T. Song, T.X. Shen, L.H. Shen, J. Xiao, H.M. Gu, Fuel 104 (2013) 244–252.
[38] K. Shah, B. Moghtaderi, T. Wall, Energy Fuels 26 (4) (2012) 2038–2045.
[39] J. Yang, N. Cai, Z.J. Li, Energy Fuels 22 (4) (2008) 2570–2579.
[40] H. Zhao, L. Liu, B. Wang, D. Xu, L. Jiang, C. Zheng, Energy Fuels 22 (2) (2008) 898–905.
[41] H. Zhao, K. Wang, Y. Fang, J. Ma, D. Mei, C. Zheng, Int. J. Greenhouse Gas Control 22 (2014) 154–164.
[42] W.J. Yang, H.B. Zhao, K. Wang, C.G. Zheng, Proc. Combust. Inst. 35 (2015) 2811–2818.
[43] W.J. Yang, H.B. Zhao, J.C. Ma, D.F. Mei, C.G. Zheng, Energy Fuels 28 (6) (2014) 3970–3981.
[44] Y.X. Zhang, E. Doroodchi, B. Moghtaderi, Energy Fuels 29 (1) (2015) 337–345.
[45] H.R. Kim, D. Wang, L. Zeng, S. Bayham, A. Tong, E. Chung, M.V. Kathe, S. Luo, O. McGiveron, A. Wang, Z. Sun, D. Chen, L.S. Fan, Fuel 108 (2013) 370–384.
[46] M. Johansson, T. Mattisson, A. Lyngfelt, A. Abad, Fuel 87 (6) (2008) 988–1001.
[47] W. Chunbo, W. Jinxing, L. Ming, G. Haining, Energy Fuels 27 (2013) 6185–6190.
[48] H. Leion, T. Mattisson, A. Lyngfelt, Fuel 86 (12–13) (2007) 1947–1958.